Multilayer modal method for diffraction gratings of arbitrary profile, depth, and permittivity

Lifeng Li

Optical Sciences Center, University of Arizona, Tucson, Arizona 85721

Received March 18, 1993; revised manuscript received June 1, 1993; accepted June 2, 1993

A numerically stable method is presented for the analysis of diffraction gratings of arbitrary profile, depth, and permittivity in conical mountings. It is based on the classical modal method and uses a stack of lamellar grating layers to approximate an arbitrary profile. A numerical procedure known as the R-matrix propagation algorithm is used to propagate the modal fields through the layers. This procedure renders the implementation of this new method completely immune to the numerical instability that is associated with the conventional propagation algorithm. Numerical examples including diffraction efficiencies of both dielectric and metallic gratings of depths that range from subwavelength to hundreds of wavelengths are presented. Information about the convergence and the computation time of the method is also included.

1. INTRODUCTION

In an earlier paper[1] I generalized the classical modal method[2,3] for lamellar gratings in nonconical mountings to conical mountings. In this paper I further extend this method to gratings of arbitrary profiles. It is well known that an arbitrary grating profile can be approximated by a stack of lamellar gratings. This technique is called the multilayer approximation, and henceforth the method that uses the multilayer approximation and the modal method to solve grating problems will be called here the multilayer modal method (MMM). The multilayer approximation was first suggested by Peng *et al.*,[4] and it has been used by numerous authors.[5–8]

In the MMM Maxwell's equations are solved in terms of modal field expansions in each layer, and the solutions in different layers are connected by the boundary conditions. In practice, in order to achieve a sufficient numerical accuracy, one must retain a large number of modal fields in the field expansions. Owing to the presence of exponential functions with large positive and negative exponents, numerical instabilities often arise when the solutions are propagated through the layers. This problem has prevented previous authors from successfully implementing the MMM that is based on the classical modal method. Suratteau *et al.*[5] presented one version of the MMM. Their numerical implementation required data clipping: any number smaller than x_m or greater than x_M is replaced by x_m, or x_M, respectively, but no unambiguous criteria for choosing x_m and x_M were given. Lee and George[6] presented a similar version of the MMM, and they encountered numerical instability for a three-layered metallic grating as the groove depth-to-period ratio h/d approached 0.2. It should be mentioned, however, that there are other realizations of the MMM that apparently do not suffer from the above-mentioned numerical instabilities. For example, the coupled-wave method[7] can treat sinusoidal or triangular dielectric gratings of h/d values up to 4. Recently, Pai and Awada[8] introduced a new method for dielectric gratings in the TE polarization. The method uses multiple-reflection matrix series to compute diffraction efficiencies. They claimed that their method was stable for gratings of arbitrary profile and thickness.

The novelty of the present study is the way in which the modal field expansions are propagated through the layers of lamellar gratings. This propagation method is borrowed from the chemical-physics literature. It is called the R-matrix propagation algorithm,[9,10] which apparently is well known in the field of chemical physics but little known in the fields of optics and electromagnetics. The essence of this algorithm is to propagate, instead of the unknown field amplitudes, a scalar or a matrix that links the unknown field amplitudes to their derivatives. In the scalar case the concept is well known in optics and microwave theory: to propagate waves through layered media, one makes use of the input impedance.[11] In the matrix case the R-matrix algorithm has been used in an extinction-theorem analysis of diffraction anomalies in overcoated gratings.[12] In this paper it is shown that the MMM that uses the R-matrix propagation algorithm is completely free of the numerical instability that occurs when the conventional propagation algorithm is used. In addition, stemming from the excellent convergence of the classical modal method for lamellar gratings,[13] my computer program can easily handle metallic gratings of arbitrary profile and depth.

In the following sections I present the mathematical details of the application of the R-matrix propagation algorithm to the multilayer lamellar grating problem. I also provide numerical examples to demonstrate the effectiveness of this method. Furthermore, a numerical convergence study is included, as well as some information about computation time. In a recent paper[14] Nevière and Popov appealed to the grating investigators to conduct further numerical experiments to evaluate the new method of Pai and Awada[8] for small wavelength-to-period ratio, metallic gratings, and TM polarization. Although the present paper is different from that of Ref. 8, I have considered the comments of Nevière and Popov in the evaluation of my new method. In order to keep the paper to a manage-

0740-3232/93/122581-11$06.00

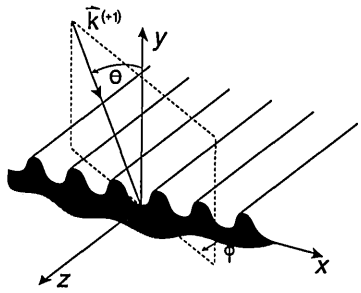

Fig. 1. Coordinate system for a diffraction grating in a conical mounting.

able size, I have referred the reader frequently to Ref. 1 for mathematical details of the modal method for lamellar gratings.

2. MATHEMATICAL FORMULATION

A. Notation

A diffraction grating in a conical diffraction configuration is depicted in Fig. 1. A monochromatic plane wave of vacuum wavelength λ is incident on the grating at a polar angle θ and an azimuthal angle ϕ. The range of θ is $0 \le \theta < \pi/2$, and that of ϕ is $-\pi < \phi \le \pi$, with the clockwise direction being the positive direction for ϕ. The same conventions will be used for the diffracted waves that are not shown in the figure. The incident polarization is, in general, elliptical.

Figure 2 shows how a general grating is approximated by a multilayer lamellar grating and various notations. I label the layered media from bottom to top and denote the interface between the jth and $(j+1)$th layers by y_j, $j = 0, 1, 2, \ldots, M$. The zeroth and $(M+1)$th layers are the two semi-infinite media. In this paper the integer M is called the stratification order. For numerical reasons to be made clear in Appendix B, I also introduce a fictitious interface y_{-1} within medium 0 such that $y_{-1} < y_0$. The abscissas $x_{l,j}$, $l = 1, 2$, are defined such that the grating profile bisects the vertical lines. The thickness of the jth layer is, in general, dependent on j and is given by

$$h_j = y_j - y_{j-1}, \quad j = 0, 1, \ldots, M. \tag{1}$$

The permittivities may also depend on j, but within each layer they are piecewise constant:

$$\epsilon_j(x) = \begin{cases} \epsilon_{2,j}, & x_{1,j} \le x \le x_{2,j}, \\ \epsilon_{1,j}, & \text{otherwise} \end{cases} \qquad j = 1, 2, \ldots, M. \tag{2}$$

To reveal the symmetry of the electric and magnetic fields, I formally assume that the permeabilities are coordinate dependent in this section, so an expression similar to Eq. (2) can be written for $\mu_j(x)$.

I denote by $k_j(x)$ the magnitudes of the wave vector in layers $j = 0, 1, \ldots, M+1$:

$$k_j^2(x) = \epsilon_j(x)\mu_j(x)k^2, \qquad j = 0, 1, \ldots, M+1, \tag{3}$$

where $k = 2\pi/\lambda$. Then the wave vector of the incident plane wave is given by

$$\mathbf{k} = k_{M+1}(\hat{x} \sin\theta \cos\phi - \hat{y} \cos\theta + \hat{z} \sin\theta \sin\phi). \tag{4}$$

I define the reduced magnitudes of the wave vectors, $\tilde{k}_j$, by

$$\tilde{k}_j^2(x) = k_j^2(x) - k_z^2, \tag{5}$$

where k_z is the z component of the incident wave vector in Eq. (4). For convenience, I will use the subscripts 0 and $M+1$ and the superscripts ± 1 interchangeably to denote ϵ, μ, k, and $\tilde{k}$ for the two exterior regions.

The time dependence and the z dependence of the form $\exp(ik_z z - i\omega t)$ for the solution of Maxwell's equations are assumed and suppressed throughout the paper. The Gaussian system of units is used.

B. Modal Field Expansion

Since the grating structure is invariant in the z direction, the grating problem can be solved in terms of only the z components of the electric and magnetic fields. The fields in the two exterior regions may be written in Rayleigh expansions:

$$\begin{pmatrix} E_z(x,y) \\ H_z(x,y) \end{pmatrix} = \begin{pmatrix} I_z^{(e)} \\ I_z^{(h)} \end{pmatrix} \exp[-i\beta_0^{(+1)} y] e_0(x) + \sum_{n=-\infty}^{+\infty} \begin{pmatrix} R_n^{(e)} \\ R_n^{(h)} \end{pmatrix} \exp[i\beta_n^{(+1)} y] e_n(x), \quad y \ge y_{M+1}, \tag{6}$$

$$\begin{pmatrix} E_z(x,y) \\ H_z(x,y) \end{pmatrix} = \sum_{n=-\infty}^{+\infty} \begin{pmatrix} T_n^{(e)} \\ T_n^{(h)} \end{pmatrix} \exp[-i\beta_n^{(-1)} y] e_n(x), \quad y \le y_0, \tag{7}$$

where

$$e_n(x) = \exp(i\alpha_n x), \tag{8}$$

$$\alpha_n = \alpha_0 + 2n\pi/d, \quad \alpha_0 = k^{(+1)} \sin\theta \cos\phi, \tag{9}$$

$$\beta_n^{(j)2} = \tilde{k}^{(j)2} - \alpha_n^2, \quad \mathrm{Re}[\beta_n^{(j)}] + \mathrm{Im}[\beta_n^{(j)}] > 0, \quad j = \pm 1. \tag{10}$$

In Eqs. (6) and (7) $I_z^{(e)}$, $I_z^{(h)}$, $R_n^{(e)}$, $R_n^{(h)}$, $T_n^{(e)}$, and $T_n^{(h)}$ are, respectively, the complex amplitudes of the z components of the incident and diffracted electric and magnetic fields in regions ± 1.

For each of the lamellar grating layers it has been proved in Ref. 1 that the total electromagnetic field can be

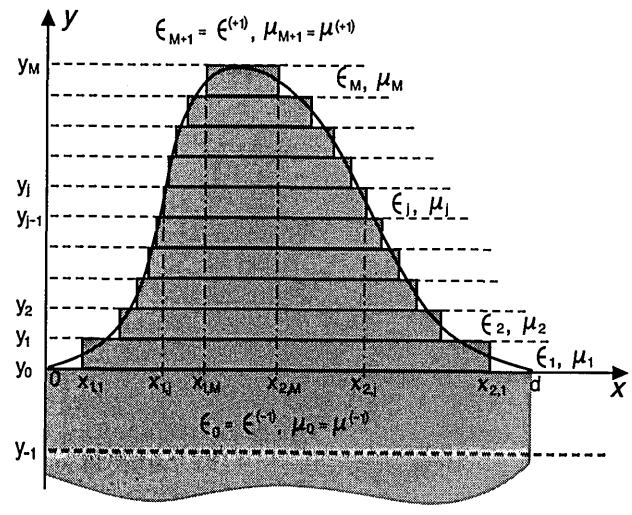

Fig. 2. Approximation of a grating of arbitrary profile by a stack of lamellar gratings.

written as a modal field expansion:

$$\begin{pmatrix} E_z(x,y) \\ H_z(x,y) \end{pmatrix} = \sum_{m=0}^{\infty} \begin{pmatrix} \omega_{m,j}^{(e)}(y) u_{m,j}^{(e)}(x) \\ \chi_{m,j}^{(e)}(y) w_{m,j}^{(e)}(x) \end{pmatrix} + \sum_{m=0}^{\infty} \begin{pmatrix} \chi_{m,j}^{(h)}(y) w_{m,j}^{(h)}(x) \\ \omega_{m,j}^{(h)}(y) u_{m,j}^{(h)}(x) \end{pmatrix}, \quad j = 1, \ldots, M. \tag{11}$$

As in Ref. 1 the superscripts (e) and (h) designate the $E_\perp$ and $H_\perp$ modes, respectively. The y dependence of a modal field is given by

$$\omega_{m,j}^{(s)}(y) = a_{m,j}^{(s)} \cos[\lambda_{m,j}^{(s)} y] + b_{m,j}^{(s)} \sin[\lambda_{m,j}^{(s)} y], \tag{12}$$

$$\chi_{m,j}^{(s)}(y) = \Lambda_{m,j}^{(s)} \{-b_{m,j}^{(s)} \cos[\lambda_{m,j}^{(s)} y] + a_{m,j}^{(s)} \sin[\lambda_{m,j}^{(s)} y]\}, \tag{13}$$

where

$$\Lambda_{m,j}^{(s)} = [k_z^2 + \lambda_{m,j}^{(s)2}]/\lambda_{m,j}^{(s)}, \quad j = 1, 2, \ldots, M, \tag{14}$$

$a_{m,j}^{(s)}$ and $b_{m,j}^{(s)}$ are the unknown modal field amplitudes, and $\lambda_{m,j}^{(s)}$ is an eigenvalue. The eigenfunctions $u_{m,j}^{(s)}(x)$ and $w_{m,j}^{(s)}(x)$ are defined in Ref. 1. As in Ref. 1 the superscript (s) stands for (e) or (h).

The Rayleigh expansions (6) and (7) can also be viewed as modal expansions. In fact, they can be cast in the form of Eq. (11), provided that one defines

$$\lambda_{m,0}^{(s)} = \beta_m^{(-1)}, \quad \lambda_{m,M+1}^{(s)} = \beta_m^{(+1)}, \tag{15}$$

$$a_{m,0}^{(s)} = T_m^{(s)}, \quad b_{m,0}^{(s)} = -iT_m^{(s)}, \tag{16}$$

$$a_{m,M+1}^{(s)} = R_m^{(s)} + I_z^{(s)} \delta_{m0}, \quad b_{m,M+1}^{(s)} = i[R_m^{(s)} - I_z^{(s)} \delta_{m0}], \tag{17}$$

$$u_{m,j}^{(s)}(x) = e_m(x), \quad w_{m,j}^{(s)}(x) = 0, \quad j = 0, M+1. \tag{18}$$

In addition, I extend the definition of $\chi_{m,j}^{(s)}(y)$ to $j = 0$, $M + 1$ by using Eqs. (16), (17), and

$$\Lambda_{m,j}^{(s)} = i, \quad j = 0, M+1. \tag{19}$$

These notations permit the layers of finite and semi-infinite thicknesses to be treated in a unified fashion in the following subsections.

C. Sector Transfer Matrix

Having obtained the modal field expansions for all the layers, I am ready to connect them together by applying boundary conditions at the interfaces. To proceed in an orderly fashion, I first divide the grating structure into sectors. The jth sector, $j = 0, 1, \ldots, M$, is defined to be the spatial region from $y_{j-1} + 0$ to $y_j + 0$, where the plus sign indicates the upper side of the interface. So the entire y space is divided into $M + 1$ sectors plus two semi-infinite regions $y < y_{-1}$ and $y > y_M$.

When the field propagates from one sector to another, it crosses an interface. At the interface the z and x components of the E and H fields are continuous. The x components can be easily derived from the z components [see Eqs. (57a) and (57b) in Ref. 1]. Application of the boundary conditions at the interface leads to four equations of eigenfunction expansions with the expansion coefficients as unknowns. To solve these equations, one projects all four equations onto a basis $\{u_{m,j+1}^{+(s)}(x)\}$ at the jth interface (for the definition of this basis see Ref. 1). This projection procedure leads to the infinite-dimensional matrix equation

$$\begin{pmatrix} \Omega_{j+1}(y_j + 0) \\ X_{j+1}(y_j + 0) \end{pmatrix} = \begin{bmatrix} A_{11}^{(j)} & A_{12}^{(j)} \\ A_{21}^{(j)} & A_{22}^{(j)} \end{bmatrix} \begin{pmatrix} \Omega_j(y_j - 0) \\ X_j(y_j - 0) \end{pmatrix}, \tag{20}$$

where

$$\Omega_j(y) = \begin{pmatrix} \omega_j^{(e)}(y) \\ \omega_j^{(h)}(y) \end{pmatrix}, \qquad X_j(y) = \begin{pmatrix} \chi_j^{(e)}(y) \\ \chi_j^{(h)}(y) \end{pmatrix}. \tag{21}$$

Each entry on the right-hand sides of Eqs. (21) is an infinite-dimensional vector. For example, $\omega_j^{(e)}(y)$ has components $\omega_{m,j}^{(e)}(y), m = 0, 1, \ldots$. The expressions for the block matrices $A_{11}^{(j)}$, etc., are not given here because they are not important to the subsequent discussion.

To complete the solution propagation within one sector, I write down the readily verifiable relation

$$\begin{pmatrix} \Omega_j(y_j - 0) \\ X_j(y_j - 0) \end{pmatrix} = \begin{bmatrix} C_{11}^{(j)} & -S_{12}^{(j)} \\ S_{21}^{(j)} & C_{22}^{(j)} \end{bmatrix} \begin{pmatrix} \Omega_j(y_{j-1} + 0) \\ X_j(y_{j-1} + 0) \end{pmatrix}, \tag{22}$$

where

$$C_{11}^{(j)} = C_{22}^{(j)} = \begin{bmatrix} \cos[\lambda_{m,j}^{(e)} h_j] & 0 \\ 0 & \cos[\lambda_{m,j}^{(h)} h_j] \end{bmatrix}, \tag{23}$$

$$S_{12}^{(j)} = \begin{bmatrix} [1/\Lambda_{m,j}^{(e)}] \sin[\lambda_{m,j}^{(e)} h_j] & 0 \\ 0 & [1/\Lambda_{m,j}^{(h)}] \sin[\lambda_{m,j}^{(h)} h_j] \end{bmatrix}, \tag{24}$$

$$S_{21}^{(j)} = \begin{bmatrix} \Lambda_{m,j}^{(e)} \sin[\lambda_{m,j}^{(e)} h_j] & 0 \\ 0 & \Lambda_{m,j}^{(h)} \sin[\lambda_{m,j}^{(h)} h_j] \end{bmatrix}. \tag{25}$$

In Eqs. (23)–(25) the nonzero matrix elements represent diagonal matrices with m running through all nonnegative integers. Substituting Eq. (22) into Eq. (20), we have

$$\begin{pmatrix} \Omega_{j+1}(y_j + 0) \\ X_{j+1}(y_j + 0) \end{pmatrix} = \begin{bmatrix} t_{11}^{(j)} & t_{12}^{(j)} \\ t_{21}^{(j)} & t_{22}^{(j)} \end{bmatrix} \begin{pmatrix} \Omega_j(y_{j-1} + 0) \\ X_j(y_{j-1} + 0) \end{pmatrix}, \tag{26}$$

where

$$\begin{bmatrix} t_{11}^{(j)} & t_{12}^{(j)} \\ t_{21}^{(j)} & t_{22}^{(j)} \end{bmatrix} = \begin{bmatrix} A_{11}^{(j)} & A_{12}^{(j)} \\ A_{21}^{(j)} & A_{22}^{(j)} \end{bmatrix} \begin{bmatrix} C_{11}^{(j)} & -S_{12}^{(j)} \\ S_{21}^{(j)} & C_{22}^{(j)} \end{bmatrix}. \tag{27}$$

I call matrix $t^{(j)}$ the transfer matrix or simply the t matrix for sector j. The sector t matrix propagates the solution vector from the lower end of a sector to the upper end.

D. T-Matrix Propagation Algorithm

At this point the direction for the rest of the derivation seems to be straightforward. Since Eq. (26) is a recursion formula, one could easily relate the field amplitudes at $y_j + 0$ to those at $y_{-1} + 0$ by defining a global T matrix, $T^{(j)}$, such that

$$T^{(j)} = t^{(j)} t^{(j-1)} \cdots t^{(0)}. \tag{28}$$

In particular, one could use the global T matrix $T^{(M)}$ to set up a system of linear equations and thereby solve for the diffraction amplitudes in the two exterior regions. This is the algorithm adopted in Refs. 4 and 5. Note that there is an apparent advantage in this algorithm, in that it does not involve matrix inversions.

Unfortunately, the algorithm as presented in Eq. (28) leads to numerical instability. Table 1 illustrates the numerical instability for a simple symmetrical two-layer lamellar grating when the T-matrix propagation algorithm is implemented in double precision on a computer. In this

Table 1. Illustration of the Numerical Instability of the *T*-Matrix Propagation Algorithm[a]

N	R_{-1}	T_{-1}	e_Σ
5	0.40296(−2)	0.34246	0.203(−1)
13	0.33724(−2)	0.33892	0.128(−3)
21	0.33710(−2)	0.33888	0.879(−5)
29	0.33405(−2)	0.33865	−0.184(−3)
37	0.20989	0.89279(−5)	0.809(−1)
45	0.72681(+2)	0.11770(−6)	0.171(+3)
Exact	0.33706(−2)	0.33888	−0.122(−14)

[a] R_{-1} and T_{-1} are diffraction efficiencies, and e_Σ is the sum of the efficiencies minus one. The integers in parentheses are base-ten exponents. The grating is symmetrical. The plane wave is incident normally and TE polarized. Other values of the parameters are $\epsilon^{(+1)} = 1.0$, $\epsilon^{(-1)} = (1.65)^2$, $\lambda = 0.6328d$, $h_1 = h_2 = 0.25d$, $x_{2,1} - x_{1,1} = 0.6d$, and $x_{2,2} - x_{1,2} = 0.2d$.

table and throughout this paper the number of terms, N, in the modal expansions that are kept for the computation is called the truncation order. The exact values in the last row are computed with an algorithm to be described in Subsection 2.E. A stable numerical method should produce ever increasingly accurate diffraction efficiency values as the truncation order increases. It can be seen from the table that the efficiency values initially converge to the exact values as N increases, but then they diverge quickly away from the exact values as N increases further. Suppose a truncation order is optimal if it yields the best approximation to the exact solution. Then it can be shown that the optimal truncation order is inversely proportional to the grating groove depth. So, although the T-matrix propagation algorithm may yield satisfactory results for shallow gratings, it completely fails for deep gratings because an unreasonably low truncation order leads to a poor numerical accuracy. In addition, my numerical experimentation showed that, for a given groove depth, the numerical instability cannot be removed by an increase in the number of lamellar layers.

The authors of Refs. 4 and 5 used exponential functions $\exp(\pm i\lambda y)$ instead of the functions $\omega_{m,j}^{(s)}(y)$ and $\chi_{m,j}^{(s)}(y)$. However, this difference does not change the numerical instability because the two sets of functions are related by a linear transformation, and hence their solution propagator is related to mine by a trivial similarity transformation.

E. *R*-Matrix Propagation Algorithm

The solution to the numerical instability problem actually has been in existence for quite some time in the field of chemical physics.[9,10] It is called the R-matrix propagation method. The choice of the letter R is for historical reasons. It should not be confused with the diffraction amplitudes in Eq. (6). In what follows, I briefly outline this simple and powerful technique as it applies to the MMM.

The matrix equation (26) can be rearranged into the form

$$\begin{pmatrix} \Omega_j(y_{j-1} + 0) \\ \Omega_{j+1}(y_j + 0) \end{pmatrix} = \begin{bmatrix} r_{11}^{(j)} & r_{12}^{(j)} \\ r_{21}^{(j)} & r_{22}^{(j)} \end{bmatrix} \begin{pmatrix} X_j(y_{j-1} + 0) \\ X_{j+1}(y_j + 0) \end{pmatrix}, \tag{29}$$

where

$$\begin{bmatrix} r_{11}^{(j)} & r_{12}^{(j)} \\ r_{21}^{(j)} & r_{22}^{(j)} \end{bmatrix} = \begin{bmatrix} -t_{21}^{(j)-1} t_{22}^{(j)} & t_{21}^{(j)-1} \\ t_{12}^{(j)} - t_{11}^{(j)} t_{21}^{(j)-1} t_{22}^{(j)} & t_{11}^{(j)} t_{21}^{(j)-1} \end{bmatrix}. \tag{30}$$

The matrix defined above is called the sector r matrix for sector j. The expressions of the sector r matrices for the nonconical case are given in Appendix B. Next, I introduce the global R matrix such that

$$\begin{pmatrix} \Omega_0(y_{-1} + 0) \\ \Omega_{j+1}(y_j + 0) \end{pmatrix} = \begin{bmatrix} R_{11}^{(j)} & R_{12}^{(j)} \\ R_{21}^{(j)} & R_{22}^{(j)} \end{bmatrix} \begin{pmatrix} X_0(y_{-1} + 0) \\ X_{j+1}(y_j + 0) \end{pmatrix}. \tag{31}$$

It is easy to show that the block elements of the global R matrix obey a set of recursion formulas as follows:

$$\begin{aligned} R_{11}^{(j)} &= R_{11}^{(j-1)} + R_{12}^{(j-1)} Z^{(j)} R_{21}^{(j-1)}, \\ R_{12}^{(j)} &= -R_{12}^{(j-1)} Z^{(j)} r_{12}^{(j)}, \\ R_{21}^{(j)} &= r_{21}^{(j)} Z^{(j)} R_{21}^{(j-1)}, \\ R_{22}^{(j)} &= r_{22}^{(j)} - r_{21}^{(j)} Z^{(j)} r_{12}^{(j)}, \end{aligned} \tag{32}$$

where

$$Z^{(j)} = [r_{11}^{(j)} - R_{22}^{(j-1)}]^{-1}. \tag{33}$$

The R-matrix propagation process comprises the calculation of the sector r matrix for each sector by Eq. (30) and the propagation of the global R matrix to the next sector by Eqs. (32). One can initialize by setting

$$\begin{bmatrix} R_{11}^{(0)} & R_{12}^{(0)} \\ R_{21}^{(0)} & R_{22}^{(0)} \end{bmatrix} = \begin{bmatrix} r_{11}^{(0)} & r_{12}^{(0)} \\ r_{21}^{(0)} & r_{22}^{(0)} \end{bmatrix}. \tag{34}$$

The propagation process is completed when the global R matrix $R^{(M)}$ is obtained. From Eq. (31), with $j = M$, a system of linear equations that relates the diffraction amplitudes in the two exterior regions to the incident plane wave can be easily derived:

$$\begin{bmatrix} 1 + R_{11}^{(M)} & -R_{12}^{(M)} \\ R_{21}^{(M)} & 1 - R_{22}^{(M)} \end{bmatrix} \begin{pmatrix} \tilde{T} \\ \tilde{R} \end{pmatrix} = \begin{bmatrix} -1 + R_{11}^{(M)} & -R_{12}^{(M)} \\ R_{21}^{(M)} & -1 - R_{22}^{(M)} \end{bmatrix} \begin{pmatrix} 0 \\ \tilde{I} \end{pmatrix}, \tag{35}$$

where

$$\begin{aligned} \tilde{I} &= \begin{pmatrix} I_z^{(e)} \\ I_z^{(h)} \end{pmatrix} \delta_{m0} \exp[-\beta_m^{(+1)} y_M], \\ \tilde{R} &= \begin{pmatrix} R_m^{(e)} \\ R_m^{(h)} \end{pmatrix} \exp[i\beta_m^{(+1)} y_M], \\ \tilde{T} &= \begin{pmatrix} T_m^{(e)} \\ T_m^{(h)} \end{pmatrix} \exp[-i\beta_m^{(-1)} y_{-1}]. \end{aligned} \tag{36}$$

Each vector entry in Eqs. (36) should be understood as a vector, and the exponential functions should be understood as diagonal matrices. Equation (35) can be numerically solved with standard techniques.

When the diffraction efficiencies in medium 0 are not of interest or when they do not exist, as in the case of a metallic grating, an alternative initialization method can be used. Since there is no incident wave coming from below the grating, $\omega_{m,j}^{(s)}(y) = -\chi_{m,j}^{(s)}(y)$ for all $y < y_0$. One can therefore set

$$\begin{bmatrix} R_{11}^{(-1)} & R_{12}^{(-1)} \\ R_{21}^{(-1)} & R_{22}^{(-1)} \end{bmatrix} = \begin{bmatrix} -1 & 0 \\ 0 & -1 \end{bmatrix}, \tag{37}$$

and, by the recursion formulas in Eqs. (32), $R_{12}^{(j)} = R_{21}^{(j)} = 0$ and $R_{11}^{(j)} = -1$ for all $j \geq 0$. Thus, effectively, only the 22

block of the full global R matrix needs to be propagated, and Eq. (35) reduces to

$$[1 - R_{22}^{(M)}]\tilde{R} = -[1 + R_{22}^{(M)}]\tilde{I}. \tag{38}$$

(In this case R_{22} is the matrix analog of the impedance or the admittance, depending on the incident polarization, of the scalar case.) When this second initialization method is used, the information about the transmitted diffraction orders is lost, but a considerable saving in computation time can be gained if only the reflected diffraction orders are needed. An example of this time saving is given in Subsection 3.C.

The R-matrix algorithm has previously been applied to the diffraction grating problem in Ref. 12. There are two differences between the present study and that of Ref. 12. First, the fundamental analytical methods on which the R-matrix algorithm is applied are different: the present paper uses the modal method, while Ref. 12 uses the extinction-theorem method. Consequently, the former is stable, but the latter is unstable for gratings of large depth-to-period ratio.[15] Second, in Ref. 12 only the second initialization method [Eq. (37)] is used.

A detailed analysis of why the T-matrix propagation algorithm is numerically unstable and why the R-matrix propagation algorithm is stable is beyond the scope of this paper. However, three important points should be mentioned here: (1) the T-matrix propagation algorithm propagates the two linearly independent solutions of Maxwell's equations, while the R-matrix propagation algorithm propagates the R matrix, which acts like a ratio between these two (infinite-dimensional vector) solutions. (2) In the numerical implementation of the R-matrix algorithm it is crucial that the analytical expressions of the sector r matrix be used; otherwise, numerical instability could arise (see Appendix B). (3) Contrary to what is commonly believed, the numerical instability associated with the T-matrix propagation algorithm is not due to underflow or overflow, at least not when double precision is used; rather, it is due to the finite precision of the number representation. In fact, the numerical instability that is illustrated in Table 1 develops long before underflow or overflow occurs.

F. Diffraction Efficiency and Polarization

Suppose that the media in regions 0 and $M + 1$ are lossless and that the incident plane wave is normalized such that

$$[\beta_0^{(+1)}/\tilde{k}^{(+1)2}][\epsilon^{(+1)}|I_z^{(e)}|^2 + \mu^{(+1)}|I_z^{(h)}|^2] = 1. \tag{39}$$

Then the diffraction efficiencies for the reflected and transmitted propagating waves of order n are given by

$$\eta_n^{(+1)} = [\beta_n^{(+1)}/\tilde{k}^{(+1)2}][\epsilon^{(+1)}|R_n^{(e)}|^2 + \mu^{(+1)}|R_n^{(h)}|^2], \tag{40}$$

$$\eta_n^{(-1)} = [\beta_n^{(-1)}/\tilde{k}^{(-1)2}][\epsilon^{(-1)}|T_n^{(e)}|^2 + \mu^{(-1)}|T_n^{(h)}|^2], \tag{41}$$

respectively. If the media in the grating region are also lossless, the sum of the efficiencies should be unity (the energy-balance theorem).

In many applications involving conical mountings it is very important to be able to predict the states of polarization of the diffracted orders. For each propagating order with wave vector

$$\mathbf{k}_n^{(j)} = \hat{x}\alpha_n + \hat{y}\,\mathrm{sgn}(j)\beta_n^{(j)} + \hat{z}k_z, \quad j = \pm 1, \tag{42}$$

one can associate two unit vectors $\hat{s}_n^{(j)}$ and $\hat{p}_n^{(j)}$, such that

$$\hat{s}_n^{(j)} = [\mathbf{k}_n^{(j)} \times \hat{y}]/|\mathbf{k}_n^{(j)} \times \hat{y}|, \qquad \hat{p}_n^{(j)} = \hat{s}_n^{(j)} \times \mathbf{k}_n^{(j)}/k^{(j)}. \tag{43}$$

The polarization of this diffracted order can be described by the two angular parameters

$$\alpha_n^{(j)} = \arctan[|E_{ns}^{(j)}|/|E_{np}^{(j)}|], \quad 0 \le \alpha_n^{(j)} \le \pi/2,$$

$$\delta_n^{(j)} = -\arg[E_{ns}^{(j)}/E_{np}^{(j)}], \qquad -\pi < \delta_n^{(j)} \le \pi, \tag{44}$$

where $E_{ns}^{(j)}$ and $E_{np}^{(j)}$ are the s and p components of the electric field, respectively. [The notation $\alpha_n^{(j)}$ should not be confused with α_n defined in Eq. (9)]. It is a simple exercise to show that, for a diffracted wave in medium $M + 1$,

$$\frac{E_{ns}^{(+1)}}{E_{np}^{(+1)}} = \left[\frac{\mu^{(+1)}}{\epsilon^{(+1)}}\right]^{1/2} \frac{\alpha_n \epsilon^{(+1)} k_0 R_n^{(e)} + \beta_n^{(+1)} k_z R_n^{(h)}}{\alpha_n \mu^{(+1)} k_0 R_n^{(h)} - \beta_n^{(+1)} k_z R_n^{(e)}}. \tag{45}$$

From Eq. (45) one may obtain the expression for a diffracted wave in medium 0 by replacing $R_n^{(s)}$ by $T_n^{(s)}$, superscript (+1) by (−1), and $\beta_n^{(+1)}$ by $-\beta_n^{(-1)}$. In this paper I

Table 2. Comparison of the Numerical Results of the Present Study and the Results of Chuang and Kong[16] for a Sinusoidal Dielectric Grating in a Conical Mounting[a]

Diffraction Order	$I_z^{(h)} = 0$		$I_z^{(e)} = 0$	
	Chuang and Kong	Present Paper	Chuang and Kong	Present Paper
R_{-3}	0.1121(−1)	0.11230(−1)	0.2076(−1)	0.20818(−1)
R_{-2}	0.3738(−1)	0.37471(−1)	0.3564(−1)	0.35725(−1)
R_{-1}	0.3875(−1)	0.38568(−1)	0.7006(−2)	0.70720(−2)
R_0	0.1032	0.10300	0.1071(−1)	0.10716(−1)
T_{-5}	0.1555(−3)	0.19070(−3)	0.3122(−3)	0.49460(−3)
T_{-4}	0.2934(−4)	0.25231(−4)	0.4914(−3)	0.59074(−3)
T_{-3}	0.7523(−2)	0.74235(−2)	0.1637(−1)	0.16219(−1)
T_{-2}	0.4893(−1)	0.49520(−1)	0.9429(−1)	0.96267(−1)
T_{-1}	0.9950(−1)	0.99081(−1)	0.1676	0.16902
T_0	0.7127(−1)	0.71571(−1)	0.4624(−1)	0.46401(−1)
T_1	0.5181	0.51845	0.5597	0.55621
T_2	0.6381(−1)	0.63408(−1)	0.4108(−1)	0.40467(−1)
Sum	1.0000	0.99993	1.0000	1.00000

[a]The case is taken from Tables 1 and 2 of Ref. 16. The incident wave vector forms a 75° angle with the z axis, and its projection in the x–y plane forms a 60° angle with the y axis. Other values of the parameters are $\epsilon^{(-1)}/\epsilon^{(+1)} = 4.0$, $d/\lambda = 2.0$, $h/\lambda = 0.6$, $M = 50$, and $N = 41$.

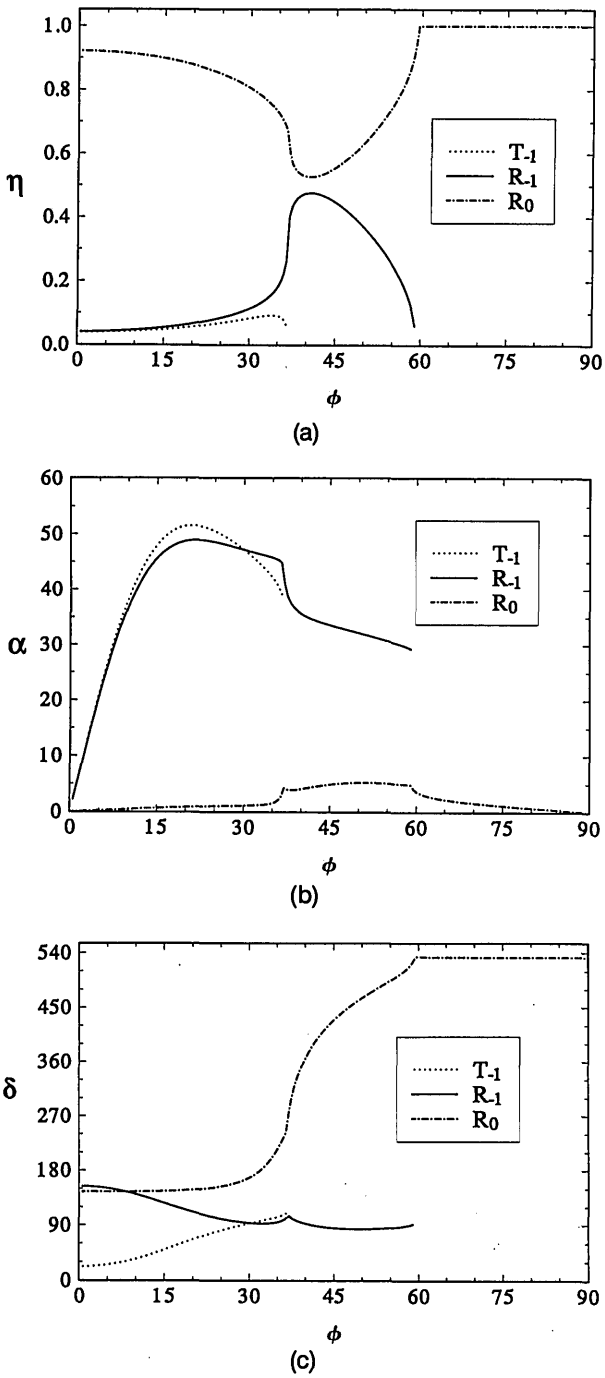

Fig. 3. (a) Efficiencies and (b) and (c) polarization angles of the diffraction orders generated by a sinusoidal grating as functions of the incident azimuthal angle ϕ. The incident polar angle is 60°, and the incident polarization is p. Other values of parameters are $d = 0.3$ μm, $h = 0.15$ μm, $\epsilon^{(+1)} = 2.25$, $\epsilon^{(-1)} = 1.0$, $\lambda = 0.5$ μm, $M = 30$, and $N = 31$.

speak of s and p polarizations when the grating is in a conical mounting and of TE and TM polarizations if the grating is in the classical mounting ($\phi = 0$).

3. NUMERICAL RESULTS

A. Numerical Examples

For simplicity, the MMM that uses the R-matrix propagation algorithm and the classical modal method[1-3] is henceforth called the R-matrix MMM. The computer program used for this study, based on the R-matrix MMM, has been checked with the energy-balance and reciprocity criteria and compared favorably with many published numerical data. In this subsection I present several examples to demonstrate the capability of the R-matrix MMM and the stability of the R-matrix propagation algorithm. In all the examples it is assumed that $h_j = h/M$, $\epsilon_{1j} = \epsilon^{(+1)}$, and $\epsilon_{2j} = \epsilon^{(-1)}$ and that the magnetic permeability is unity everywhere.

In Table 2 the numerical results of the present study for the diffraction efficiencies of a sinusoidal dielectric grating in a conical mounting are compared with those of Chuang and Kong,[16] who used the extended boundary condition method. The two incident polarizations are chosen such that the magnetic-field and electric-field vectors are perpendicular to the z axis, respectively. The agreement between these two methods is, in general, very good.

In Fig. 3 the diffraction efficiencies and the polarization angles are presented as functions of the incident azi-

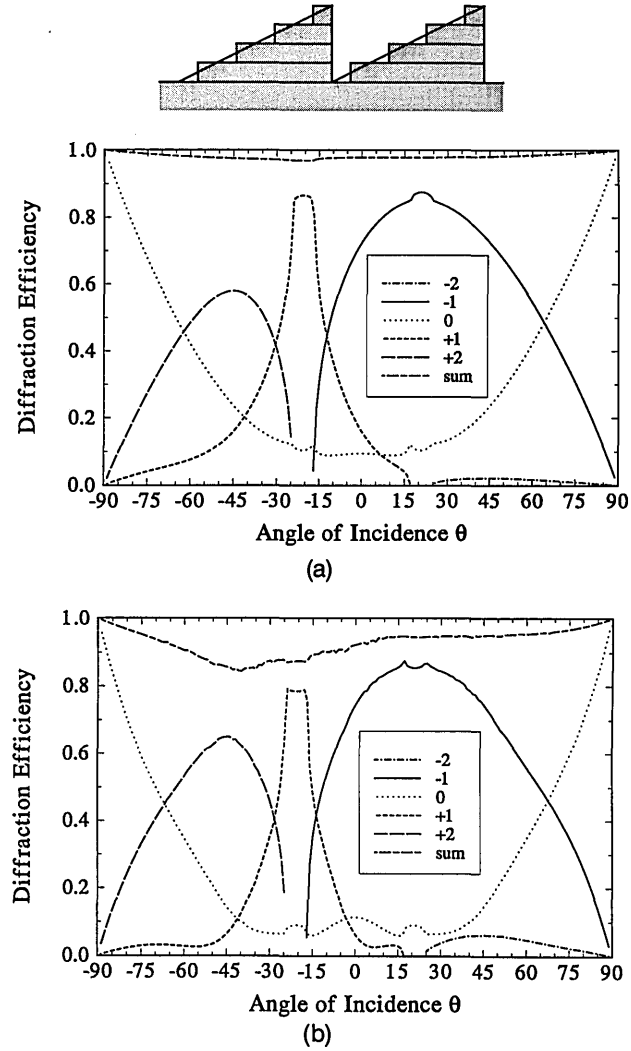

Fig. 4. Diffraction efficiencies of a silver four-level binary grating in (a) TE and (b) TM polarizations. The binary grating approximates a right-angle triangular grating whose period is 0.8233 μm and whose depth is 0.341 μm. Other values of parameters are $\epsilon^{(+1)} = (1.46)^2$, $\epsilon^{(-1)} = (0.1 + i5.58)^2$, $\lambda = 0.85$ μm, and $N = 51$. Here $\theta < 0$ is equivalent to $\theta > 0$ and $\phi = 180°$ in the polar coordinate system that is defined in Fig. 1.

Table 3. Diffraction Efficiencies of Sinusoidal Dielectric Gratings of Four Groove Depth-to-Period Ratios[a]

Diffraction Order	$h/d = 0.1$		$h/d = 1.0$		$h/d = 10$	$h/d = 100$
	MMM	RFM	MMM	IM	MMM	MMM
			(a) TE Polarization			
R_{-2}	0.61092(−3)	0.60804(−3)	0.33921(−2)	0.417(−2)	0.95722(−3)	0.11639(−2)
R_{-1}	0.96767(−2)	0.96660(−2)	0.76680(−3)	0.945(−3)	0.17554(−3)	0.77516(−3)
R_0	0.41656(−1)	0.41686(−1)	0.20552(−2)	0.256(−2)	0.14991(−2)	0.10110(−2)
T_{-3}	0.70696(−5)	0.67940(−5)	0.19936(−1)	0.173(−1)	0.29696(−2)	0.16525(−2)
T_{-2}	0.46550(−4)	0.45917(−4)	0.15202	0.145	0.49744	0.19831
T_{-1}	0.16766(−1)	0.16740(−1)	0.49591	0.496	0.41107	0.79592(−1)
T_0	0.87272	0.87282	0.20795	0.211	0.67499(−1)	0.68959
T_1	0.58522(−1)	0.58430(−1)	0.11798	0.128	0.18383(−1)	0.27908(−1)
			(b) TM Polarization			
R_{-2}	0.77607(−3)	0.76830(−3)	0.17302(−2)	0.145(−2)	0.58514(−4)	0.19653(−2)
R_{-1}	0.91238(−2)	0.90746(−2)	0.66721(−3)	0.816(−3)	0.12167(−5)	0.21009(−3)
R_0	0.14948(−1)	0.14876(−1)	0.18662(−3)	0.306(−3)	0.10463(−3)	0.24559(−3)
T_{-3}	0.78879(−5)	0.52827(−5)	0.12821(−1)	0.122(−1)	0.64171(−3)	0.41496(−2)
T_{-2}	0.59184(−4)	0.59931(−4)	0.21339	0.212	0.18693	0.13827
T_{-1}	0.14850(−1)	0.14826(−1)	0.46158	0.464	0.27573	0.85497(−1)
T_0	0.93539	0.93586	0.18362	0.186	0.52608	0.75031
T_1	0.24849(−1)	0.24527(−1)	0.12600	0.127	0.10448(−1)	0.19358(−1)

[a]The values of the parameters are $\epsilon^{(+1)} = 1.0$, $\epsilon^{(-1)} = 2.25$, $\theta = 30°$, $\phi = 0$, $d/\lambda = 1.7$, $M = 50$, and $N = 41$. MMM stands for the present multilayer modal method, RFM stands for the Rayleigh–Fourier method, and IM stands for the integral method.

Table 4. Diffraction Efficiencies of Sinusoidal Metallic Gratings of Four Groove Depth-to-Period Ratios[a]

Diffraction Order	$h/d = 0.1$		$h/d = 1.0$		$h/d = 10$	$h/d = 100$
	MMM	RFM	MMM	IM	MMM	MMM
			(a) TE Polarization			
R_{-2}	0.01160	0.01155	0.41348	0.422	0.19932	0.07331
R_{-1}	0.20667	0.20635	0.33531	0.329	0.13715	0.02018
R_0	0.76020	0.76079	0.20177	0.199	0.30096	0.01711
			(b) TM Polarization[b]			
R_{-2}	0.0279	0.02697	0.1264	0.157	0.0494	0.0057
R_{-1}	0.2784	0.27655	0.0603	0.079	0.3307	0.0164
R_0	0.6519	0.66037	0.6609	0.566	0.1618	0.0747

[a]The values of the parameters are $\epsilon^{(+1)} = 1.0$, $\epsilon^{(-1)} = (0.3 + i7.0)^2$, $\theta = 30°$, $\phi = 0$, $d/\lambda = 1.7$, $M = 50$, and $N = 51$. MMM stands for the present multilayer modal method, RFM stands for the Rayleigh–Fourier method, and IM stands for the integral method.
[b]Same parameter values as in (a), except that $M = 10$ and $N = 105$.

muthal angle ϕ for a sinusoidal dielectric grating when a p-polarized plane wave is incident from the optically denser medium. This configuration is known to simulate what happens when a TM-polarized guided wave propagates in a periodically corrugated planar waveguide with its propagation direction noncollinear to the grating vector.[17] The reflected and transmitted negative first orders pass off at approximately $\phi = 37°$ and $\phi = 60°$, respectively. It is evident that as soon as ϕ is nonzero, the two diffraction orders become (right-handed) elliptically polarized. Three similar figures for a lamellar grating have been presented in Ref. 1.

The multilayer method is naturally suited for analysis of binary diffraction gratings. In Fig. 4 diffraction efficiencies of a four-level silver grating are presented as functions of incident angle θ. For this grating the TE and TM diffraction characteristics are quite similar. In particular, the two negative first-order diffraction efficiency curves are nearly identical, and they hold high values over a wide range of angles of incidence. Note that although the grating profile is asymmetrical, the zero-order efficiency curves are symmetrical with respect to $\theta = 0$, as required by the reciprocity theorem.

Next, I present numerical results of diffraction efficiencies for dielectric sinusoidal gratings in the TE and TM polarizations in Table 3, (a) and (b), respectively, and for metallic sinusoidal gratings in the TE and TM polarizations in Table 4, (a) and (b), respectively. The grating groove depths are shallow ($h/d = 0.1$), deep ($h/d = 1.0$), very deep ($h/d = 10$), and extremely deep ($h/d = 100$). At optical wavelengths the last two groove depths are difficult to achieve (if at all) with current technology. They are included here merely to demonstrate the stability of the R-matrix MMM in the extreme situations. The refractive index of the metallic gratings is chosen to correspond to gold or silver at a wavelength of approximately 1 μm. In addition, taking the comments of Nevière and Popov in Ref. 14 into consideration, I have chosen the grating period-to-wavelength ratio to be 1.7 to permit eight propagating orders for the dielectric gratings and three propagating orders for the metallic gratings.

For the shallowest gratings ($h/d = 0.1$) I have included

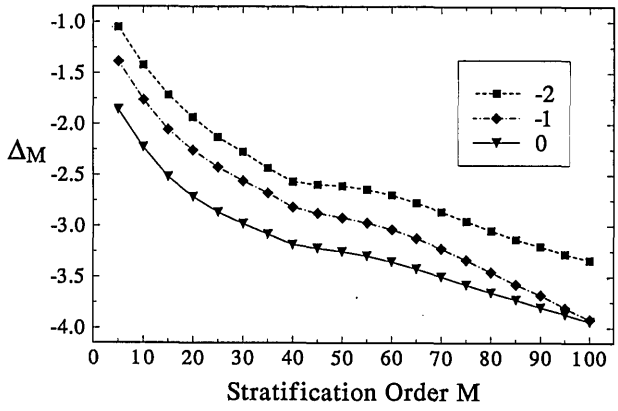

Fig. 5. Convergence of the TE diffraction efficiencies with respect to the stratification order M for a shallow metallic grating [the first grating in Table 4; $h/d = 0.1$]. $M^* = 170$.

efficiency values computed by the Rayleigh–Fourier method,[15] which is perfectly capable of giving accurate results for this h/d value. For the next greater groove depth ($h/d = 1.0$) I have included the results of the integral method.[18] At this depth the Rayleigh–Fourier method is no longer applicable, but the integral method is still capable of producing reliable results, although it begins to have convergence difficulties. The agreement between my MMM and these two methods is very good at these two depths. The next two greatest groove depths are far beyond the reach of the integral method and any other grating methods. Therefore I do not have an independent numerical method for checking the accuracies of the efficiency values for these two depths; future authors are invited to do so.

B. Convergence

To demonstrate further the excellent stability of the R-matrix MMM, I now examine the convergence of the diffraction efficiencies with respect to the stratification order M and the truncation order N, taking the diffraction efficiencies in Tables 3 and 4 as examples. For this purpose a measure of error is defined as follows:

$$\Delta_q = \log_{10}|(f_q - f_{q^*})/f_{q^*}|, \tag{46}$$

where q is an integer that can represent either M or N, $q^* \gg q$ is another integer, and f_q is a physical quantity such as diffraction efficiency computed at q. Roughly speaking, the magnitude of Δ_q gives the number of correct digits in the numerical results. Without this sensitive measure most of the curves to be presented below would become horizontal lines.

Based on physical intuition, one can expect that as the thickness of the stratified grating layers decreases, the diffraction efficiencies of the multilayer grating should converge to the efficiencies of the grating being approximated. Figure 5 gives an example of this convergence process for the shallowest metallic grating in Table 4, (a). Physical intuition also suggests that in order for a multilayer lamellar grating structure to approximate accurately an arbitrary grating profile, the thickness of each layer must be considerably less than the wavelength of the incident light. This point is demonstrated in Fig. 6, where the diffraction efficiencies for the second deepest grating in Table 4, (a), are given as functions of the stratification order. Clearly, the efficiency values stabilize only when the layer thickness is less than half a wavelength. Thus the stratification orders used for the last two columns of Tables 3 and 4 are not large enough for modeling the sinusoidal gratings. The efficiency values listed there should be understood as the values of the approximating gratings rather than the values of the sinusoidal gratings that are being approximated.

In principle, the convergence of diffraction efficiencies with respect to the stratification order does not represent the intrinsic convergence characteristics of the MMM. Each stratification order corresponds to a realistic grating structure, which has its own definite diffraction efficiencies. How well the MMM converges with respect to M depends on how well the grating profile can be approximated by a small number of rectangular layers. The intrinsic convergence of the MMM should be measured with respect to the truncation order N.

Figures 7 and 8 show the convergence of the diffraction efficiencies of the transmitted negative first orders of the four dielectric gratings in Table 3 and the reflected negative first orders of the four metallic gratings in Table 4, respectively. As with other methods the R-matrix MMM converges much faster for dielectric gratings than for metallic gratings, and it also converges much faster for the TE polarization then for the TM polarization. In general, the convergence is excellent. Even for the most difficult case of deep metallic gratings in the TM polarization, convergence is achieved. The convergence for the dielectric gratings in both polarizations and for the metallic gratings in the TE polarization is very fast. To achieve 1% accuracy for dielectric gratings, one needs to keep only 11 modal fields. To achieve the same accuracy for metallic gratings, one needs to keep 35 and 65 modal fields for the TE and TM polarizations, respectively.

In the case of lossless dielectric gratings in nonconical mountings our computer program always produces very small errors (of the order of 10^{-14}) in the sum of diffraction efficiencies, even when the truncation order is less than the total number of the propagating orders. This fact clearly indicates that somehow the energy-balance theorem is automatically satisfied by the R-matrix propagation algorithm. In the case of conical mountings, how-

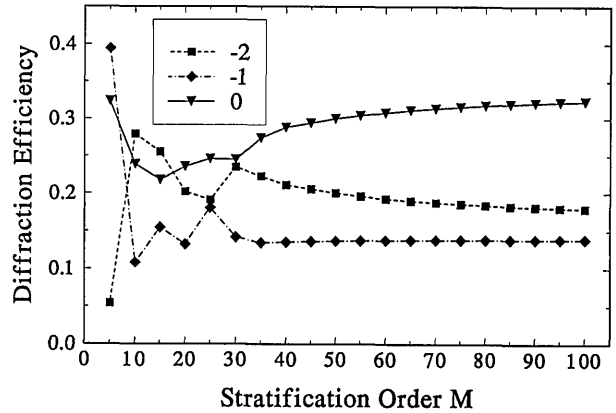

Fig. 6. Convergence of the TE diffraction efficiencies with respect to the stratification order M for a very deep metallic grating [the third grating in Table 4; $h/d = 10$].

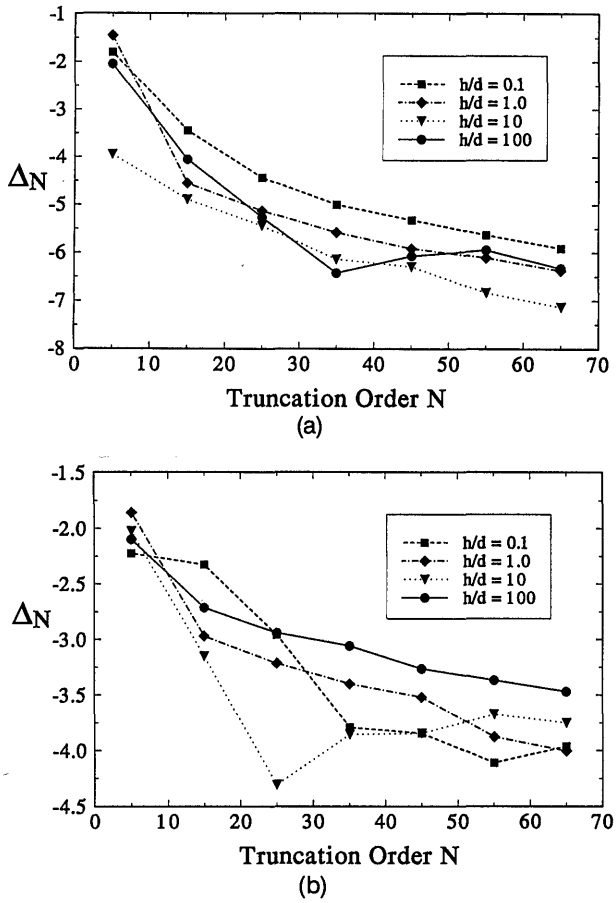

Fig. 7. (a) Convergence of the transmitted negative first-order TE diffraction efficiencies for the four dielectric gratings referenced in Table 3. $N^* = 105$. (b) Convergence of the transmitted negative first-order TM diffraction efficiencies for the four dielectric gratings referenced in Table 3. $N^* = 105$.

ever, the theorem is not automatically satisfied, which is already evident in Table 2. The difference between these two cases originates in the way that the Mth-sector r matrix is calculated (see Appendix B).

One of the most interesting features of the R-matrix MMM is that its convergence with respect to N is practically independent of the grating groove depth. To achieve the same accuracy, a shallow grating and an extremely deep grating require the same matrix size and therefore the same computation time, provided that the stratification orders are the same. For other methods, such as the integral method and the differential method, the required matrix dimension increases as the grating groove depth increases.[11] For these methods the required matrix dimension increases as the grating groove depth increases.

C. Computation Time

For a given grating diffraction problem the computation time T required of the R-matrix MMM is essentially a function of the truncation order N and the stratification order M. The form of this function, $T(M, N)$, can be estimated as follows. Because of the recursive nature of the R-matrix propagation algorithm, T can be expected to be proportional to M. The computation time for finding N eigenvalues and eigenfunctions is proportional to N, and the computation time for assembling various matrices is proportional to N^2. The computation time for the matrix operations such as matrix multiplications and inversions is proportional to N^3. Therefore

$$T = a + MP_3(N), \tag{47}$$

where P_3 is a third-degree polynomial and a is a small constant representing overheads such as input and output.

In Fig. 9 the actual timing results are presented for computing diffraction efficiencies of the gratings referenced in Tables 3 and 4 on a workstation (SPARCstation 2, SPARC International, Inc., Mountain View, Calif.). Since the grating depth does not explicitly enter Eq. (47), each set of data in Fig. 9 is valid for any one of the columns under heading MMM in the corresponding table. It can be seen that all six sets of data are fit very well by Eq. (47). In general, the computation of dielectric gratings takes less time than that of metallic gratings, but the TE polarization case does not necessarily take less time than the TM polarization case. Note that when N is large, the second initialization method [Eq. (37)] results in considerable savings in computation time compared with the first initialization method [Eq. (34)]. For the sake of clarity, the timing results for conical mountings are not shown in Fig. 9. Since a conical mounting takes matrices twice as large as those taken by a nonconical mounting, it can be expected that the computation time for the former is approximately eight times that for the latter when N is large.

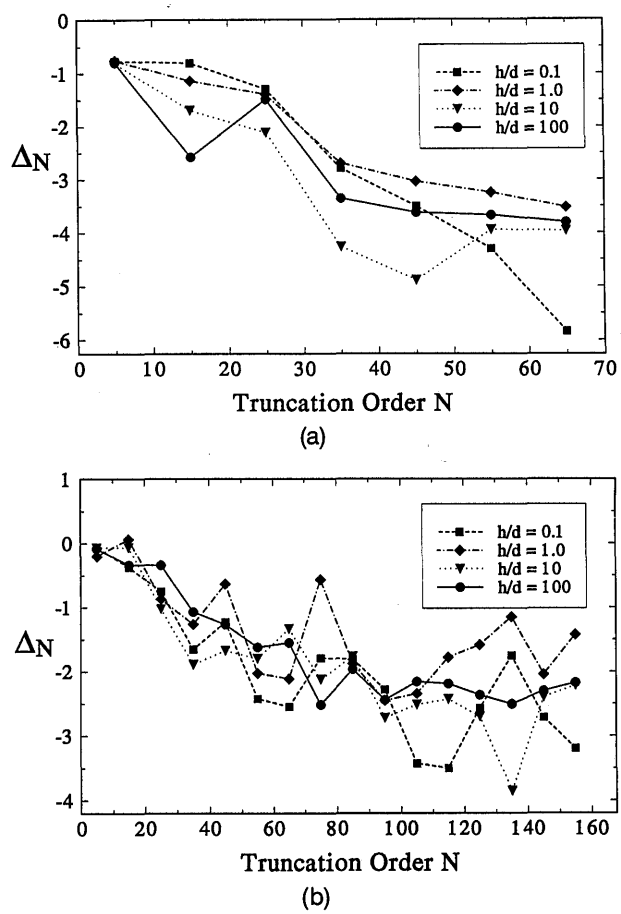

Fig. 8. (a) Convergence of the negative first-order TE diffraction efficiencies for the four metallic gratings referenced in Table 4. $N^* = 105$. (b) Convergence of the negative first-order TM diffraction efficiencies for the four metallic gratings referenced in Table 4. $N^* = 195$.

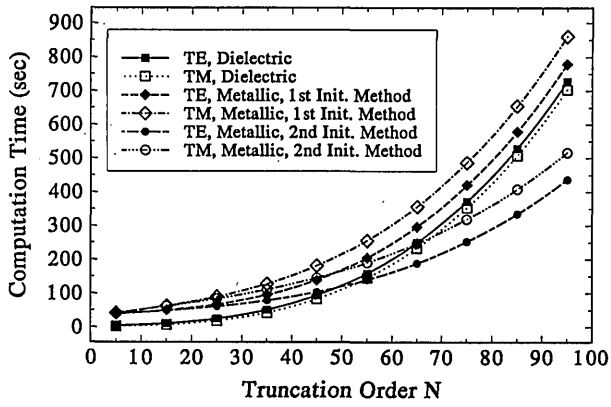

Fig. 9. Computation times for computing diffraction efficiencies of the gratings referenced in Tables 3 and 4. The CPU times were measured with a SPARCstation 2 made by SPARC International, Inc. The computer program runs in double precision. The stratification order is fixed at $M = 10$. The curves are the third-order polynomial fits.

Since the convergence of the R-matrix MMM with respect to N is independent of the groove depth and M is proportional to the groove depth for deep gratings, then, for a given accuracy requirement, the computation time is directly proportional to the groove depth when the depth is large. In contrast, the computation time for other methods increases rapidly (more than linear dependence) with the groove depth.

4. SUMMARY

I have presented a new multilayer modal method (MMM) that is based on the classical modal method and the R-matrix propagation algorithm. The numerical examples that have been presented in Section 3 demonstrate the excellent convergence and stability of this method. I have presented some numerical results for deep dielectric and metallic gratings that previously could not be modeled by other methods. With this new MMM no numerical instability has been experienced that is associated with the evanescent and antievanescent waves of large exponents, even for gratings of extremely deep grooves. I have also provided some information on the convergence and the computation time of this new method.

Because of its use of the multilayer approximation the MMM is applicable to gratings of arbitrary surface relief profile and gratings that have a gradient index of refraction in the y direction. The multilayer approximation offers the MMM its flexibility and, at the same time, its inefficiency in treating smooth grating profiles. For smooth grating profiles of moderate depth other grating methods such as the integral method and the Rayleigh method are much more efficient. Only for lamellar gratings and gratings of shape or depth beyond the reach of the other methods does the MMM prove to be advantageous. In this sense the MMM and the other existing methods are complementary.

The MMM can be trivially extended to treat gratings buried within a planar multilayered structure. In principle, the MMM can also be extended to treat coated (multiple curved surfaces) gratings, although, based on the comment in the previous paragraph, it will be inefficient. Moreover, in this case the application of the multilayer approximation leads to a permittivity function that has more than two discontinuities per grating period for a given y, and the modal analysis in Ref. 1 must be modified.

Like any numerical method the R-matrix MMM surely has its own limitations. The reader might have noticed that I have kept the stratification order M small for the metallic gratings in the TM polarization. I have found that when M is greater than 15 or so, the computed diffraction efficiencies do not converge, but they do not diverge either. As M or N increases, the efficiency values fluctuate around the correct values predicted by the Rayleigh–Fourier method and the integral method when they are applicable. In addition, the sum of efficiencies is always less than unity, as it should be for metallic gratings. At present, the real cause of this type of numerical instability is unknown, and the analysis of highly conducting gratings of arbitrary profiles in the TM polarization remains a challenging problem.

APPENDIX A: ELEMENTARY MATRICES

In this appendix I define the elementary matrix elements that are used in the expressions of the sector r matrices in Appendix B. They have the general form

$$\langle f|q|g\rangle = \int_0^d \overline{f(x)} q(x) g(x) \mathrm{d}x, \tag{A1}$$

where f and g are the eigenfunctions $e_n(x)$ and $u_{m,j}^{(s)}(x)$ and q is a weight function. If $q = 1$, it is omitted in the notation on the left-hand side of Eq. (A1). One can easily obtain the analytical expressions of the elementary matrix elements by performing integration by parts twice and by the use of the differential equations that the eigenfunctions obey.

Because the eigenfunctions are orthonormal and complete, as has been discussed in Ref. 1, there exist certain relations among these elementary matrices. For example,

$$[\langle e_m^+|1/\epsilon_1|u_{n,1}^{(h)}\rangle]^{-1} = [\langle u_{m,1}^{+(h)}|e_n\rangle], \tag{A2}$$

$$[\langle u_{m,j}^{+(h)}|1/e_{j+1}|u_{n,j+1}^{(h)}\rangle]^{-1} = [\langle u_{m,j+1}^{+(h)}|1/\epsilon_j|u_{n,j}^{(h)}\rangle], \tag{A3}$$

where the superscript + denotes the adjoint eigenfunctions and the square brackets denote the matrices with the representative elements enclosed.

APPENDIX B: SECTOR r MATRICES

For simplicity, I give the expressions of the sector r matrices for only the TM polarization case. In this case the matrices are contracted to half the size of those in the conical mounting case. The sector matrices $\mathrm{r}^{(j)}$ take three forms depending on whether $j = 0$, $0 < j < M$, or $j = M$.

For $j = 0$,

$$r_{11}^{(0)} = i\delta_{mn} \cot[\beta_n^{(-1)} h_0],$$

$$r_{12}^{(0)} = \frac{\epsilon^{(-1)}}{\beta_m^{(-1)}} \csc[\beta_m^{(-1)} h_0] \left\langle e_m^+ \left| \frac{1}{\epsilon_1} \right| u_{n,1}^{(h)} \right\rangle,$$

$$r_{21}^{(0)} = i \left\langle u_{m,1}^{+(h)} \left| \frac{1}{\epsilon_1} \right| e_n \right\rangle \csc[\beta_n^{(-1)} h_0],$$

$$r_{22}^{(0)} = \sum_{l=0}^{\infty} \left\langle u_{m,1}^{+(h)} \left| \frac{1}{\epsilon_1} \right| e_l \right\rangle \frac{\epsilon^{(-1)}}{\beta_l^{(-1)}} \cot[\beta_l^{(-1)} h_0] \left\langle e_l^+ \left| \frac{1}{\epsilon_1} \right| u_{n,1}^{(h)} \right\rangle; \tag{B1}$$

for $0 < j < M$,

$$r_{11}^{(j)} = -\delta_{mn}\frac{\cot[\lambda_{n,j}^{(h)}h_j]}{\lambda_{n,j}^{(h)}},$$

$$r_{12}^{(j)} = \frac{\csc[\lambda_{m,j}^{(h)}h_j]}{\lambda_{m,j}^{(h)}}\left\langle u_{m,j}^{+(h)}\left|\frac{1}{\epsilon_{j+1}}\right|u_{n,j+1}^{(h)}\right\rangle,$$

$$r_{21}^{(j)} = -\left\langle u_{m,j+1}^{+(h)}\left|\frac{1}{\epsilon_{j+1}}\right|u_{n,j}^{(h)}\right\rangle\frac{\csc[\lambda_{n,j}^{(h)}h_j]}{\lambda_{n,j}^{(h)}},$$

$$r_{22}^{(j)} = \sum_{l=0}^{\infty}\left\langle u_{m,j+1}^{+(h)}\left|\frac{1}{\epsilon_{j+1}}\right|u_{l,j}^{(h)}\right\rangle\frac{\cot[\lambda_{l,j}^{(h)}h_j]}{\lambda_{l,j}^{(h)}}\left\langle u_{l,j}^{+(h)}\left|\frac{1}{\epsilon_{j+1}}\right|u_{n,j+1}^{(h)}\right\rangle; \tag{B2}$$

and for $j = M$,

$$r_{11}^{(M)} = -\delta_{mn}\frac{\cot[\lambda_{n,M}^{(h)}h_M]}{\lambda_{n,M}^{(h)}},$$

$$r_{12}^{(M)} = -i\frac{\beta_m^{(+1)}}{\epsilon^{(+1)}}\frac{\csc[\lambda_{m,M}^{(h)}h_M]}{\lambda_{m,M}^{(h)}}\langle u_{m,M}^{+(h)}|e_n\rangle,$$

$$r_{21}^{(M)} = -\langle e_m^{+}|u_{n,M}^{(h)}\rangle\frac{\csc[\lambda_{n,M}^{(h)}h_M]}{\lambda_{n,M}^{(h)}},$$

$$r_{22}^{(M)} = -i\sum_{l=0}^{\infty}\langle e_m^{+}|u_{l,M}^{(h)}\rangle\frac{\cot[\lambda_{l,M}^{(h)}h_M]}{\lambda_{l,M}^{(h)}}\langle u_{l,M}^{+(h)}|e_n\rangle\frac{\beta_n^{(+1)}}{\epsilon^{(+1)}}. \tag{B3}$$

The expressions for the TE polarization can be obtained simply by the replacement of ϵ by μ and superscript (h) by (e). From these expressions it is clear that a sector cannot have a zero thickness. In particular, the fictitious interface y_{-1} cannot coincide with y_0; it is otherwise arbitrary. For numerical reasons I set h_0 to be less than one wavelength in my computer program.

For the nonconical mounting I was able to derive the analytical expressions of the r matrices by using the analytical inverses of the elementary matrices that are exemplified by Eqs. (A2) and (A3). For the conical mountings I was successful in deriving analytical expressions of $r^{(j)}$ only for $0 \le j < M$. For $j = M$ I had to compute numerically the inverse of $t_{21}^{(M)}$ in order to obtain the Mth-sector r matrix. This is the reason that the energy-balance theorem is satisfied in different ways for the conical and for the nonconical mountings, as described in the text.

The following note is extremely important to a reader who plans to implement the R-matrix MMM for the conical mountings. Let us denote by λ^* the eigenvalue of the Mth sector that has the largest negative imaginary part. I observed during numerical experimentation that when $|\exp(i\lambda^* h_M)| > 10^{15}$, the numerical instability similar to that of the T-matrix propagation algorithm arose. To overcome this difficulty, I divide the Mth sectors into two subsectors such that

$$h_M = h_M' + h_M'', \quad \exp(i\lambda^* h_M'') < 10^8. \tag{B4}$$

The subsector of thickness h_M'' contains the interface y_M. To obtain the sector matrix $r^{(M)}$, one first computes the r matrices for the two subsectors separately, then combines them by using Eqs. (32). The r matrix for the singly primed subsector is given by Eqs. (22)–(25) with appropriate substitutions of notation. The r matrix for the doubly primed subsector must be computed by numerical matrix inversion and the use of Eq. (30). I have found that this procedure is very effective for removing the above-mentioned numerical instability. If $|\exp(i\lambda^* h_M)| < 10^{15}$, this procedure is not needed.

ACKNOWLEDGMENTS

This research was supported in part by the Advanced Technology Program of the U.S. Department of Commerce through a grant to the National Storage Industry Consortium.

REFERENCES

1. L. Li, "A modal analysis of lamellar diffraction gratings in conical mountings," J. Mod. Opt. **40,** 553–573 (1993).
2. L. C. Botten, M. S. Craig, R. C. Mcphedran, J. L. Adams, and J. R. Andrewartha, "The dielectric lamellar diffraction grating," Opt. Acta **28,** 413–428 (1981).
3. L. C. Botten, M. S. Craig, R. C. Mcphedran, J. L. Adams, and J. R. Andrewartha, "The finitely conducting lamellar diffraction grating," Opt. Acta **28,** 1087–1102 (1981).
4. S. T. Peng, T. Tamir, and H. L. Bertoni, "Theory of periodic dielectric waveguides," IEEE Trans. Microwave Theory Tech. **MTT-23,** 123–133 (1975).
5. J. Y. Suratteau, M. Cadilhac, and R. Petit, "Sur la détermination numérique des efficacités de certains réseaux diélectriques profonds," J. Opt. (Paris) **14,** 273–288 (1983).
6. K-T. Lee and T. F. George, "Theoretical study of laser-induced surface excitations on a grating," Phys. Rev. B **31,** 5106–5112 (1985).
7. M. G. Moharam and T. K. Gaylord, "Diffraction analysis of dielectric surface-relief gratings," J. Opt. Soc. Am. **72,** 1385–1392 (1982).
8. D. M. Pai and K. A. Awada, "Analysis of dielectric gratings of arbitrary profiles and thicknesses," J. Opt. Soc. Am. A **8,** 755–762 (1991).
9. D. J. Zvijac and J. C. Light, "R-matrix theory for collinear chemical reactions," Chem. Phys. **12,** 237–251 (1976).
10. J. C. Light and R. B. Walker, "An R-matrix approach to the solution of coupled equations for atom–molecule reactive scattering," J. Chem. Phys. **65,** 4272–4282 (1976).
11. L. M. Brekhovskikh, *Waves in Layered Media* (Academic, New York, 1960).
12. L. F. Desandre and J. M. Elson, "Extinction-theorem analysis of diffraction anomalies in overcoated gratings," J. Opt. Soc. Am. A **8,** 763–777 (1991).
13. L. Li and C. W. Haggans, "Convergence of the coupled-wave method for metallic lamellar diffraction gratings," J. Opt. Soc. Am. A **10,** 1184–1189 (1993).
14. M. Nevière and E. Popov, "Analysis of dielectric gratings of arbitrary profiles and thicknesses: comment," J. Opt. Soc. Am. A **9,** 2095–2096 (1992).
15. D. Maystre, "Rigorous vector theories of diffraction gratings," in *Progress in Optics,* E. Wolf, ed. (Elsevier Science, Amsterdam, 1984), Vol. 21, pp. 1–67.
16. S. L. Chuang and J. A. Kong, "Wave scattering from a periodic dielectric surface for a general angle of incidence," Radio Sci. **17,** 545–557 (1982).
17. L. Li, Q. Gong, G. N. Lawrence, and J. J. Burke, "Polarization properties of planar dielectric waveguide gratings," Appl. Opt. **31,** 4190–4197 (1992).
18. D. Maystre, "Integral methods," in *Electromagnetic Theory of Gratings,* Vol. 22 of Topics in Current Physics, R. Petit, ed. (Springer-Verlag, Berlin, 1980), pp. 63–100.